Mode separation in a mixed-mode I/II problem by the J-integral and higher-order theories

Balázs Kiss Phd student

Budapest University of Technology and Economics
Department of Applied Mechanics

Supervisor: Dr. András Szekrényes

Braunschweig , 2019

Contents

Composite materials

Failure mechanism of composite materials

Fiber reinforced thermoset polymer composites:

- multicomponent and multiphase materials
- high strength, high modulus reinforcement phase
- tough but stiff matrix phase

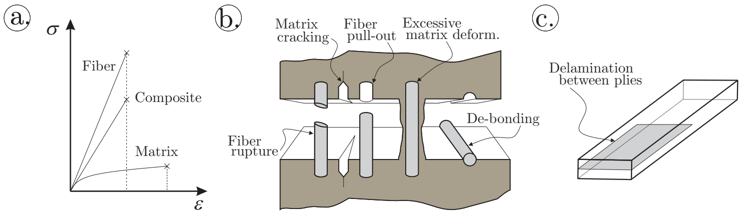

Figure 1: Tensile test of polymer composite and its components (a). Possible failure mechanism of composite materials (b-c).

Composite materials

Linear elastic fracture mechanics

Definition of the energy release rate:

$$G = -\frac{d\Pi}{dA}, \quad (1) \qquad \Pi = U - W. \quad (2)$$

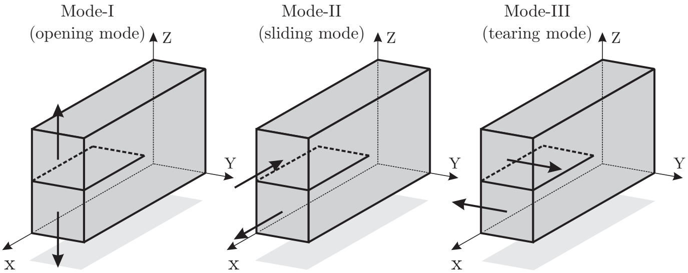

Figure 2: Basic fracture modes in linear elastic fracture mechanics.

In the case of beam-type specimens:

$$G_T = G_I + G_{II}. \quad (3)$$

Semi-layerwise beam model

Displacement field of the undelaminated region

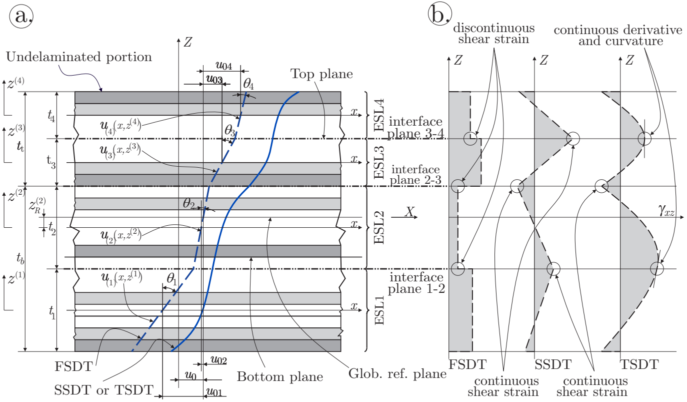

Figure 3: Cross section and the assumed deformation of the undelaminated portion in the $X-Z$ plane (a) and distributions of the transverse shear strain by different theories (b) using 4ESLs.

$$u_{(i)}(x,z^{(i)}) = u_0(x) + u_{0i}(x) + \theta_i(x)z^{(i)} + \phi_i(x)[z^{(i)}]^2 + \lambda_i(x)[z^{(i)}]^3 \qquad i = 1..4. \tag{4}$$

Definition of the stress resultants

Undelaminated region

Invariant form of the displacement fields:

$$u_{(i)} = u_0 + \left(K_{ij}^{(0)} + K_{ij}^{(1)} z^{(i)} + K_{ij}^{(2)} [z^{(i)}]^2 + K_{ij}^{(3)} [z^{(i)}]^3\right)\psi_j, \qquad i = 1..4,$$
$$w_{(i)} = w(x), \qquad i = 1..4. \tag{5}$$

Strain field:

$$\varepsilon_{x(i)} = \frac{\partial u_{(i)}}{\partial x}, \qquad \gamma_{xz(i)} = \frac{\partial u_{(i)}}{\partial z^{(i)}} + \frac{\partial w_{(i)}}{\partial x}. \tag{6}$$

Constitutive equations:

$$\begin{pmatrix} \sigma_x \\ \tau_{xz} \end{pmatrix}_{(i)} = \overline{C}_{(i)}^{(m)} \begin{pmatrix} \varepsilon_x \\ \gamma_{xz} \end{pmatrix}_{(i)} = \begin{bmatrix} E_{11}/(1-\nu_{21}\nu_{12}) & 0 \\ 0 & G_{13} \end{bmatrix}_{(i)}^{(m)} \begin{pmatrix} \varepsilon_x \\ \gamma_{xz} \end{pmatrix}_{(i)}. \tag{7}$$

Stress resultants:

$$\begin{pmatrix} N_x \\ M_x \\ L_x \\ P_x \end{pmatrix}_{(i)} = \int_0^b \int_{-t_i/2}^{t_i/2} \sigma_x \begin{pmatrix} 1 \\ z \\ z^2 \\ z^3 \end{pmatrix}_{(i)} dz^{(i)} dy, \qquad i = 1..4, \tag{8}$$

$$\begin{pmatrix} Q_{xz} \\ R_{xz} \\ S_{xz} \end{pmatrix}_{(i)} = \int_0^b \int_{-t_i/2}^{t_i/2} \tau_{xz} \begin{pmatrix} 1 \\ z \\ z^2 \end{pmatrix}_{(i)} dz^{(i)} dy, \qquad i = 1..4. \tag{9}$$

Equilibrium equations

Undelaminated region

Virtual work principle:

$$\int_{T_0}^{T_1} (\delta U - \delta W_F) dt = 0, \qquad \delta U = \sum_i \delta U_{(i)}, \qquad \delta W_F = \sum_i \delta W_{F(i)}. \tag{10}$$

Equilibrium equations of the undelaminated region:

$$\delta u_0 : \sum_{i=1}^{4} \left(\frac{\partial N_{x(i)}}{\partial x} \right) = 0, \tag{11}$$

$$\begin{aligned} \delta \psi_j : \sum_{i=1}^{4} \Bigg(& K_{ij}^{(0)} \frac{\partial N_{x(i)}}{\partial x} + K_{ij}^{(1)} \frac{\partial M_{x(i)}}{\partial x} + K_{ij}^{(2)} \frac{\partial L_{x(i)}}{\partial x} + K_{ij}^{(3)} \frac{\partial P_{x(i)}}{\partial x} - \\ & K_{ij}^{(1)} Q_{x(i)} - 2K_{ij}^{(2)} R_{x(i)} - 3K_{ij}^{(3)} S_{x(i)} \Bigg) = 0, \qquad j = 1..p, \end{aligned} \tag{12}$$

$$\delta w : \sum_{i=1}^{4} \left(\frac{\partial Q_{x(i)}}{\partial x} \right) + q = 0. \tag{13}$$

Semi-layerwise beam model

Delaminated region

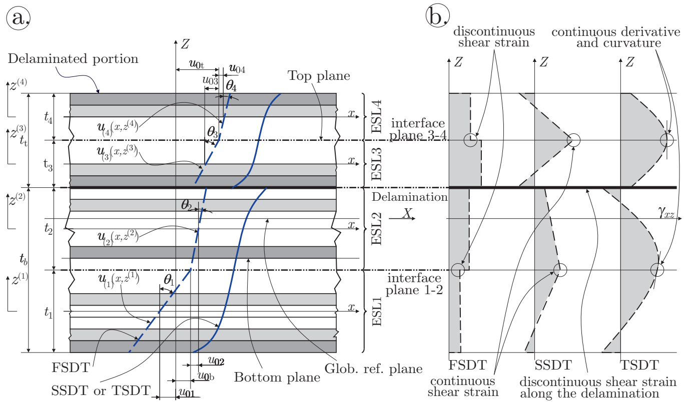

Figure 4: Cross section and the assumed deformation of the delaminated portion in the $X - Z$ plane (a) and distributions of the transverse shear strain by different theories (b) using separately 2ESLs.

$$u_{(i)}(x, z^{(i)}) = u_{0b}(x) + u_{0i}(x) + \theta_i(x)z^{(i)} + \phi_i(x)[z^{(i)}]^2 + \lambda_i(x)[z^{(i)}]^3 \qquad i = 1..2, \tag{14}$$

$$u_{(i)}(x, z^{(i)}) = u_{0t}(x) + u_{0i}(x) + \theta_i(x)z^{(i)} + \phi_i(x)[z^{(i)}]^2 + \lambda_i(x)[z^{(i)}]^3 \qquad i = 3..4. \tag{15}$$

Equlibrium equations

Delaminated portion

Invariant form of the displacement fields:

$$\begin{aligned}
u_{(i)} &= u_{0b} + \left(K_{ij}^{(0)} + K_{ij}^{(1)} z^{(i)} + K_{ij}^{(2)}[z^{(i)}]^2 + K_{ij}^{(3)}[z^{(i)}]^3\right)\psi_j, \qquad i = 1..2,\\
u_{(i)} &= u_{0t} + \left(K_{ij}^{(0)} + K_{ij}^{(1)} z^{(i)} + K_{ij}^{(2)}[z^{(i)}]^2 + K_{ij}^{(3)}[z^{(i)}]^3\right)\psi_j, \qquad i = 3..4,\\
w_{(i)} &= w_b(x), \qquad i = 1..2,\\
w_{(i)} &= w_t(x), \qquad i = 3..4.
\end{aligned} \tag{16}$$

Equilibrium equations of the delaminated portions:

$$\delta u_{0b} : \sum_{i=1}^{2}\left(\frac{\partial N_{x(i)}}{\partial x}\right) = 0, \qquad \delta u_{0t} : \sum_{i=3}^{4}\left(\frac{\partial N_{x(i)}}{\partial x}\right) = 0, \tag{17}$$

$$\begin{aligned}
\delta\psi_j : \sum_{i=1}^{4}\Bigg(&K_{ij}^{(0)}\frac{\partial N_{x(i)}}{\partial x} + K_{ij}^{(1)}\frac{\partial M_{x(i)}}{\partial x} + K_{ij}^{(2)}\frac{\partial L_{x(i)}}{\partial x} + K_{ij}^{(3)}\frac{\partial P_{x(i)}}{\partial x} -\\
&K_{ij}^{(1)} Q_{x(i)} - 2K_{ij}^{(2)} R_{x(i)} - 3K_{ij}^{(3)} S_{x(i)}\Bigg) = 0, \qquad j = 1..p,
\end{aligned} \tag{18}$$

$$\delta v_b : \sum_{i=1}^{2}\left(\frac{\partial Q_{x(i)}}{\partial x}\right) + q_b = 0, \qquad \delta v_t : \sum_{i=3}^{4}\left(\frac{\partial Q_{x(i)}}{\partial x}\right) + q_t = 0. \tag{19}$$

J-Integral

Definition and application

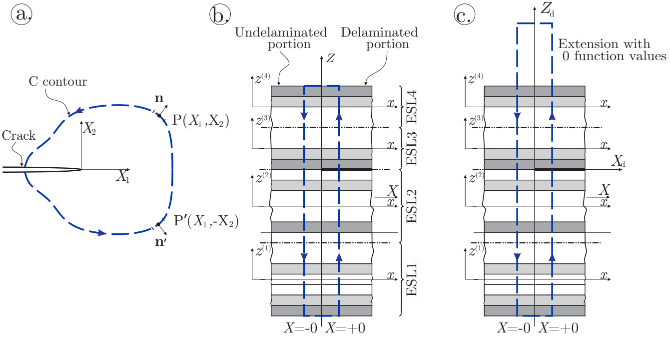

Figure 5: The general definition of the *J*-integral for in-plane problem (a). The application of the *J*-integral for semi-layerwise model using zero-area path (b) with the inevitable extension (c).

Definition of the *J*-integral:

$$J = G_T = \int_C \left\{ U n_1 - \sigma_{ij} n_j \frac{\partial u_i}{\partial x_1} \right\} ds. \tag{20}$$

J-Integral

Mode partitioning of the total J-integral

Beam-type fracture sepecimens:

$$G_T = G_I + G_{II}. \tag{21}$$

Mode-I energy release rate:

$$\begin{aligned} G_I = \int_{-t}^{+t} \Bigg\{ & \left(-\frac{1}{2}\sigma_{x(sym)}\varepsilon_{x(sym)} + \tau_{xz(ant)}\left(\frac{1}{2}\gamma_{xz(ant)} - \frac{\partial w_{(ant)}}{\partial x}\right)\right)\Bigg|_{x=-0}^{(undel)} \\ & + \left(\frac{1}{2}\sigma_{x(sym)}\varepsilon_{x(sym)} - \tau_{xz(ant)}\left(\frac{1}{2}\gamma_{xz(ant)} - \frac{\partial w_{(ant)}}{\partial x}\right)\right)\Bigg|_{x=+0}^{(del)} \Bigg\} dz_d. \end{aligned} \tag{22}$$

Mode-II energy release rate:

$$\begin{aligned} G_{II} = \int_{-t}^{+t} \Bigg\{ & \left(-\frac{1}{2}\sigma_{x(ant)}\varepsilon_{x(ant)} + \tau_{xz(sym)}\left(\frac{1}{2}\gamma_{xz(sym)} - \frac{\partial w_{(sym)}}{\partial x}\right)\right)\Bigg|_{x=-0}^{(undel)} \\ & + \left(\frac{1}{2}\sigma_{x(ant)}\varepsilon_{x(ant)} - \tau_{xz(sym)}\left(\frac{1}{2}\gamma_{xz(sym)} - \frac{\partial w_{(sym)}}{\partial x}\right)\right)\Bigg|_{x=+0}^{(del)} \Bigg\} dz_d. \end{aligned} \tag{23}$$

Built-in config.

Transversely isotropic material

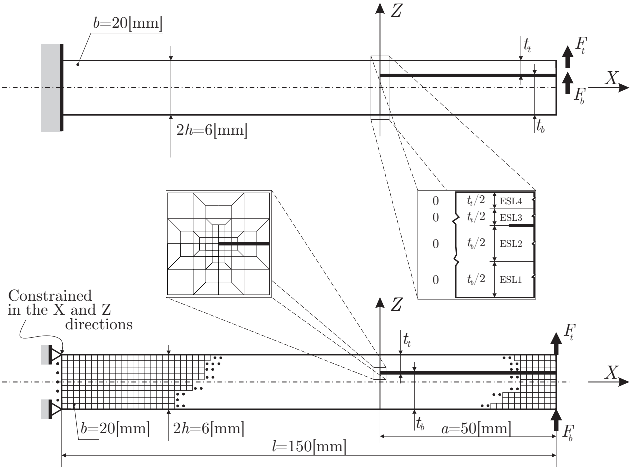

Figure 6: Built-in configuration of delaminated beam with transversely isotropic plies.

Motivation

Semi-layerwise beam model

J-Integral

Built-in config.

Mode-mixity

Transversely isotropic material

Symmetric delamination: F_t=200 N and F_b=-200 N.

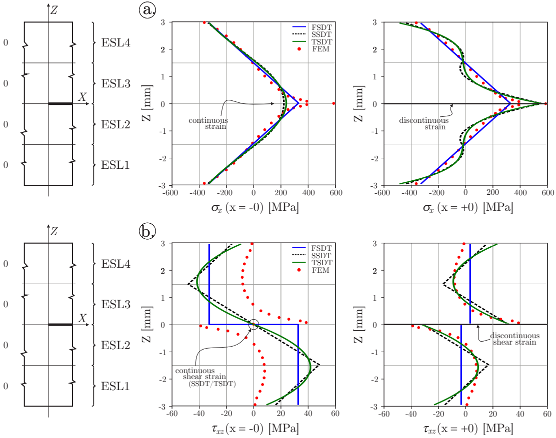

Figure 7: Distribution of the σ_x normal stresses (a) and the τ_{xz} shear stresses at the delamination tip, transversely isotropic case, $F_t = 200$ N and $F_b = -200$ N.

Transversely isotropic material

Symmetric delamination: F_t=200 N and F_b=200 N

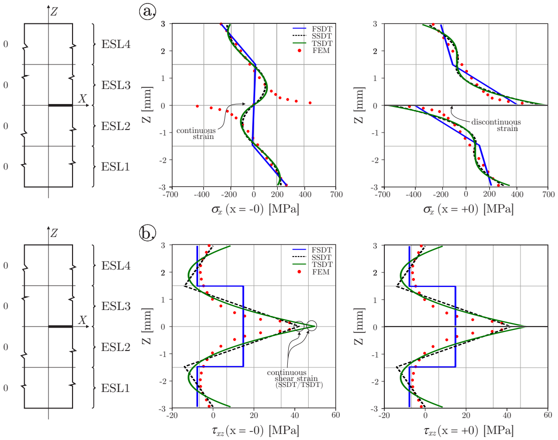

Figure 8: Distribution of the σ_x normal stresses (a) and the τ_{xz} shear stresses at the delamination tip, transversely isotropic case, F_t = 200 N and F_b = 200 N.

Energy release rates

Mode-mixity of transversely isotropic beams

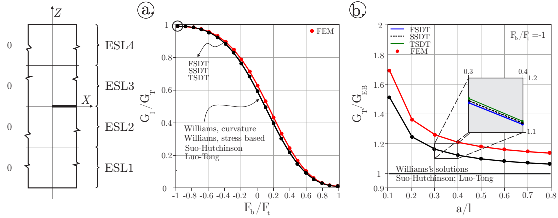

Figure 9: Mode mixity of symmetrically delaminated beam in different loading scenarios (a), $a/l = 1/3$, $2h = 6$ mm. The ratio of the G_T total and G_{EB} classical energy release rates (b), $F_b/F_t = -1$.

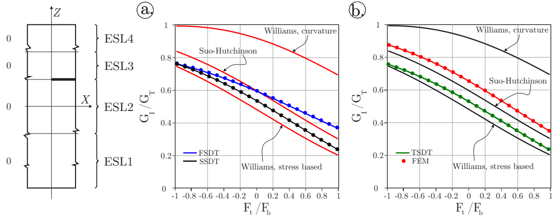

Figure 10: Mode mixity of asymmetrically delaminated beam in different loading scenarios using analytical (a) and numerical (b) solutions, $t_t/t_b = 0.5$, $a/l = 1/3$, $2h = 6$ mm.

Built-in config.

Geometry and different delamination scenarios

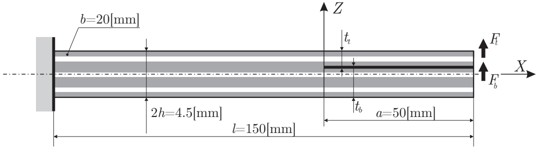

Figure 11: Built-in configuration of delaminated beam with orthotropic plies.

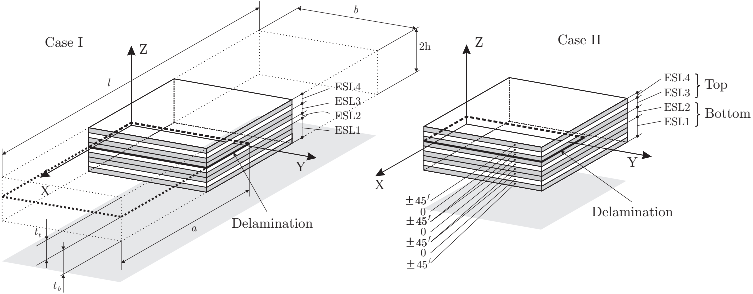

Figure 12: Different delamination scenarios of a beam element.

Results - Displacement and stress

"Case I", F_t = 10 N and F_b = -10 N

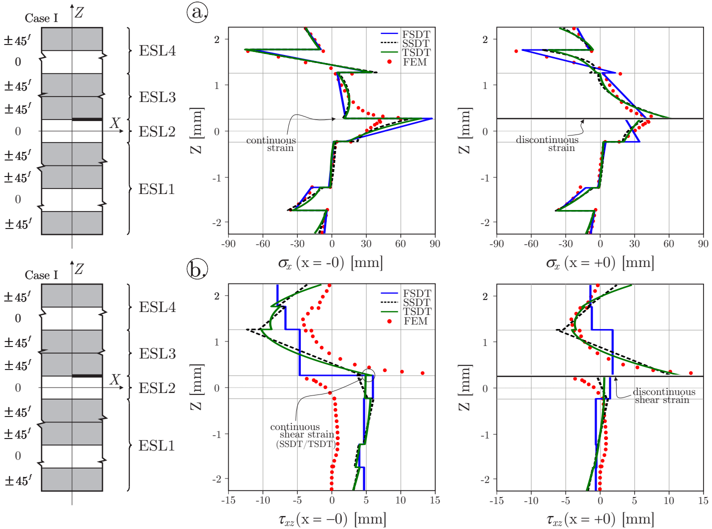

Figure 13: Distribution of the σ_x normal stresses (a) and the τ_{xz} shear stresses at the delamination tip, "Case I", F_t = 10 N and F_b = -10 N.

Energy release rates

Mode mixity

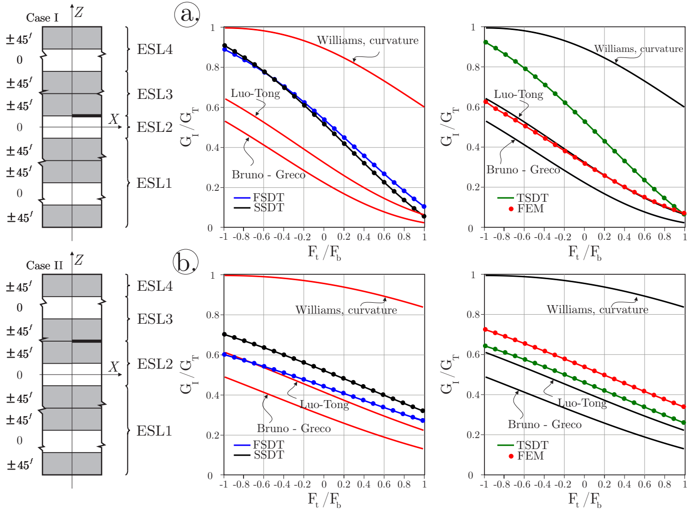

Figure 14: Mode mixity of different loading scenarios with different evaluation techniques. The delamination is located between 0 - $\pm 45^f$ layers (a) and between $\pm 45^f$ - $\pm 45^f$ layers (b), $a/l = 1/3$, $b = 20$ mm, $2h = 4.5$ mm.

Summary

- Semi-layerwise beam model
- Application of the *J*-integral
- More exact mode partitioning

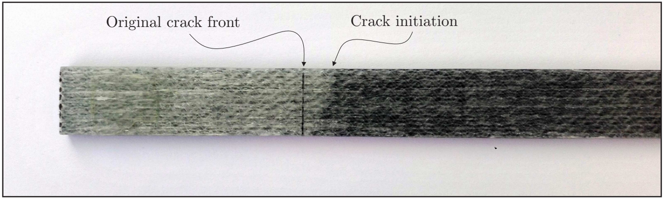

Figure 15: Straight crack front and the occured crack initiation in the of bi-material specimen.

Thank you for your attention!

The publication of the work reported herein has been supported by ETDB at BME.